JUSTC

Article

http://justc.ustc.edu.cn

Received: August 18, 2025; Accepted: March 16, 2026

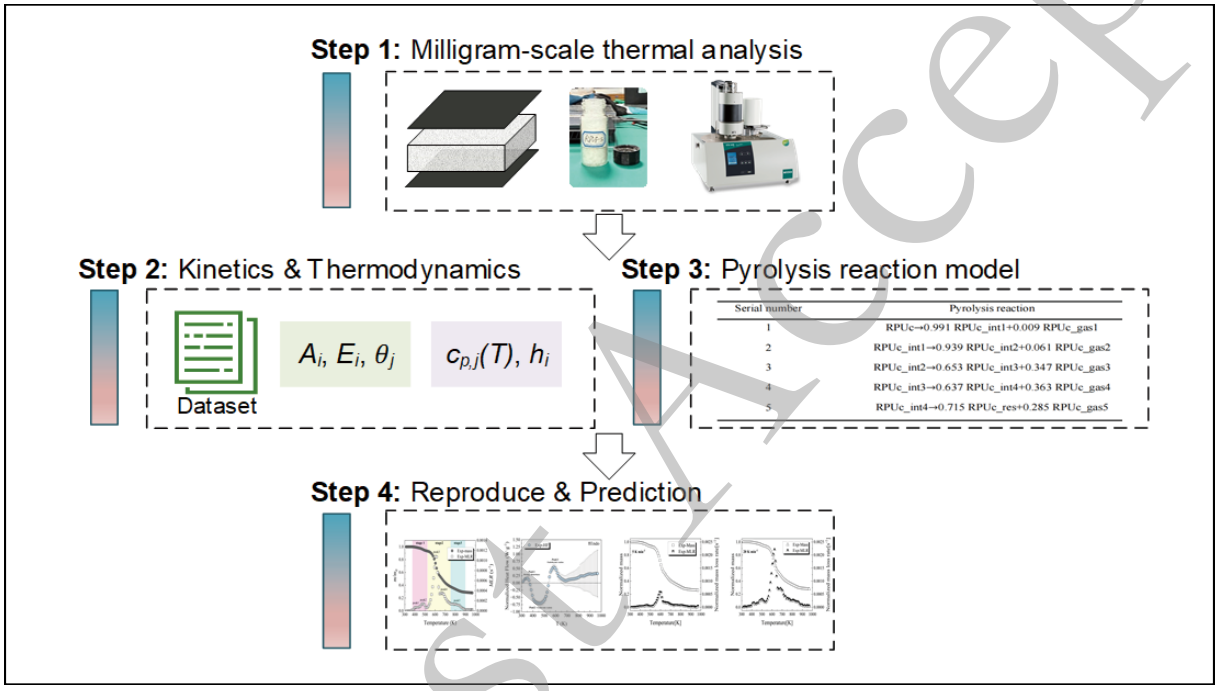
Experimental and numerical study on pyrolysis kinetics and thermodynamics of the polymer core in rigid polyurethane foam sandwich insulation materials

Xinyang Wang[1], Deyi Wang[2], Xiaowei Mu[2], Lizhong Yang[1], and Xiaoyu Ju[1] ✉

[1]*State Key Laboratory of Fire Science, University of Science and Technology of China, Jin Zhai Road 96, Hefei, Anhui, 230026 China;*
[2]*IMDEA Materials Institute, C Eric Kandel 2, 28906, Madrid, Spain*

✉Correspondence: Xiaoyu Ju, E-mail: ju.xiaoyu@ustc.edu.cn
© 2026 The Author(s). This is an open access article under the CC BY-NC-ND 4.0 license (http://creativecommons.org/licenses/by-nc-nd/4.0/).

Graphical abstract



A combined thermal analysis and numerical framework for determining pyrolysis kinetics and thermodynamics of RPUc in sandwich insulation materials.

Public summary

- Milligram-scale thermal analysis experiments were conducted on RPUc under an inert atmosphere, yielding TGA-derived mass loss and DSC-derived heat flow data during pyrolysis.
- Key pyrolysis behaviors, including the pyrolysis onset temperature, three distinct pyrolysis stages, char yield, mass loss rate, endothermic/exothermic process, and integral heat flow, were quantitatively characterized.
- A pyrolysis reaction model framework was developed to reproduce and predict the TGA and DSC data under varying heating conditions. The pyrolysis behaviors were well captured by a five-step consecutive first-order reaction mechanism with optimized thermal properties.

Citation: Wang X Y, Wang D Y, Mu X W, et al. Experimental and numerical study on pyrolysis kinetics and thermodynamics of the polymer core in rigid polyurethane foam sandwich insulation materials. *JUSTC*, **2026**, 56(0): . CSTR: 32290.14.JUSTC-2025-0084. DOI: 10.52396/JUSTC-2025-0084

Just Accepted

JUSTC

Article

http://justc.ustc.edu.cn

Received: August 18, 2025; Accepted: March 16, 2026

Experimental and numerical study on pyrolysis kinetics and thermodynamics of the polymer core in rigid polyurethane foam sandwich insulation materials

Xinyang Wang[1], Deyi Wang[2], Xiaowei Mu[2], Lizhong Yang[1], and Xiaoyu Ju[1] ✉

[1]*State Key Laboratory of Fire Science, University of Science and Technology of China, Jin Zhai Road 96, Hefei, Anhui, 230026 China;*
[2]*IMDEA Materials Institute, C Eric Kandel 2, 28906, Madrid, Spain*

✉Correspondence: Xiaoyu Ju, E-mail: ju.xiaoyu@ustc.edu.cn
© 2026 The Author(s). This is an open access article under the CC BY-NC-ND 4.0 license (http://creativecommons.org/licenses/by-nc-nd/4.0/).

Cite This: *JUSTC*, **2026**, 56(X): (9pp) Read Online SI Supporting Information

Abstract: To quantitatively characterize the pyrolysis behavior of rigid polyurethane foam core (RPUc) in sandwich insulation panels, a systematic methodology is proposed that combines thermoanalytical experiments at the milligram scale with the COMSOL Multiphysics reaction engineering module to analyze pyrolysis kinetics and thermodynamics. Mass loss profiles obtained from thermogravimetric analysis (TGA) enable the development of multi-step pyrolysis reaction mechanisms and the determination of stoichiometric coefficients, preexponential factors, and activation energies for each pyrolysis reaction via inverse modeling. A hill-climbing optimization algorithm was employed to obtain the optimal kinetic parameter set. In addition, heat flow results from differential scanning calorimetry (DSC) allow the determination of condensed-phase heat capacities and pyrolysis reaction enthalpies through inverse modeling, facilitating the development of a comprehensive pyrolysis reaction model. The results demonstrate that a five-step consecutive first-order lumped reaction mechanism successfully captures the mass loss and heat flow evolution of RPUc during pyrolysis and accurately predicts its mass loss behavior under different heating rates. The integrated methodology proposed in this study demonstrates broad applicability and can also be applied to determine the pyrolysis characteristics of combustible solids in fire-retardant sandwich panels and multi-layer polymer materials.

Keywords: Sandwich insulation core; rigid polyurethane foam; polymer pyrolysis; inverse modeling; COMSOL Multiphysics simulation

CLC number: X932; TU55^{+}1.2; TQ317.4 **Document code:** A

1 Introduction

The energy crisis[1] caused by the depletion of fossil fuel resources poses one of the greatest challenges to the global energy system in the 21st century. Governments around the world have promoted the global adoption of carbon peak and carbon neutrality policies[2, 3] to achieve energy conservation and emission reduction targets. The 2024 China Urban–Rural Development Carbon Emissions Research Report[4] indicates that in 2022, the total carbon emissions from construction and the construction industry nationwide amounted to 51.3 billion tCO_2, accounting for 48.3% of the country's energy-related carbon emissions. The total energy consumption of the national construction and construction industry was 24.2 billion tce, accounting for 44.8% of the national total energy consumption. Energy consumption in the construction industry was 12.3 billion tce, and energy consumption in building operations was 11.9 billion tce, accounting for 22.8% and 22.0% of the national total energy consumption, respectively. To reduce energy loss from buildings, façade insulation systems have been developed, wherein organic insulation materials dominate the market owing to their ultralow thermal conductivity, strong mechanical properties, simplicity of installation, and cost efficiency. Rigid polyurethane foam (RPU)[5–7] has low thermal conductivity (approximately 0.020–0.026 $W \cdot m^{-1} \cdot K^{-1}$), mechanical properties, and sound insulation properties. Therefore, it is widely used in the field of building façade insulation and is expected to account for approximately 19.8% of the market share of insulation material by 2025. In practical engineering applications, RPU insulation boards are often installed in building exterior insulation systems in the form of sandwich panels. The top and bottom surface layers are typically made of metal or inorganic materials, such as aluminum foil or cement mortar fiber paper, while the core material is RPU with added flame retardants. Nevertheless, the inherent flammability of organic materials has led to frequent fire incidents in building façade insulation systems, particularly in high-rise buildings[8–10]. Therefore, systematically evaluating the fire hazard of this sandwich insulation material is vital for providing theoretical and data support for the design of energy-efficient and safe organic exterior wall insulation materials.

Extensive studies have investigated the pyrolysis and combustion behavior of rigid polyurethane foam core (RPUc) in sandwich panels. Rodrigues et al.[11] compared the physical

Just Accepted

CSTR: 32290.14.JUSTC-2025-0084
DOI: 10.52396/JUSTC-2025-0084
JUSTC, **2026**, 56(X):

and thermal response characteristics of biomass-based tannin foam sandwich panels with those of conventional polyurethane foam sandwich panels through thermogravimetric analysis and SEM analysis. Proença et al.[12] conducted full-scale experimental investigations on the fire resistance performance of composite sandwich floor panels with glass fiber-reinforced polymer (GFRP) coverings and polyurethane foam cores under both standard fire scenarios and mechanical loading. The research team subsequently[13] conducted fire resistance tests of polyurethane foam-filled mesh core composite sandwich panels for building floors, considering two panel variants: (i) fully composite panels using GFRP panels and webs and (ii) hybrid panels with an additional fiber-reinforced concrete (FRC) top layer. The following characteristics were investigated: (i) temperature changes in the panel thickness, (ii) mechanical response, (iii) failure modes, and (iv) fire resistance. Wi et al.[14] conducted ignition tests on four types of polymer core materials, including polyurethane foam, using a conical heater. They evaluated the flame retardancy and combustion characteristics of four-sandwich panel polymer core materials on the basis of the ISO 13344 and ISO 19702 standards. In terms of numerical simulations of pyrolysis and combustion in sandwich panels, previous studies have focused primarily on simulation studies of the mechanical properties of sandwich panels. For instance, Feih et al.[15] and Anjang et al.[16–18] conducted modeling studies on the mechanical and water absorption properties of sandwich panels using external flames as a heat source and performed numerical analysis of the surface fracture characteristics of the latter. In recent decades, researchers have explored and developed various pyrolysis numerical models to simulate the thermal degradation and ignition of combustible solid/liquid substances such as polymers. Three comprehensive pyrolysis prediction models (Gpyro[19], the FDS solid-phase model[20], and ThermaKin2Ds[21, 22]) have gradually been developed and are currently commonly used for multidimensional numerical simulations of material pyrolysis. The first step in applying these numerical models to perform pyrolysis kinetic and thermodynamic analyses of solid materials is to obtain the required input parameters. Jiang et al.[23] employed a genetic algorithm (GA) to determine the kinetic triplets for five subreactions of polyurethane degradation in air and analyzed the effect of the isocyanate ratio on the stability of each stage. Using TG-FTIR-GC/MS, Zheng et al.[24] investigated the pyrolysis of flexible polyurethane foam and identified a three-stage degradation process linked to its key components. The shuffled complex evolution (SCE) algorithm was successfully employed to optimize the pyrolysis kinetic parameters, achieving strong agreement with the experimental data. However, current studies still lack a systematic methodology for determining simulation input parameters specific to the polymer core within sandwich insulation panels, which can be used for constructing corresponding pyrolysis reaction models and thermodynamic systems.

This work proposes a systematic methodology to characterize the pyrolysis kinetics and thermodynamics of RPUc in sandwich panels on the basis of milligram-scale thermoanalytical data and an inverse modeling approach. By coupling a lumped pyrolysis reaction mechanism with a reaction engineering framework implemented in COMSOL Multiphysics, a pyrolysis reaction model is constructed. The developed methodology provides the key input parameters required for pyrolysis modeling and offers a modeling framework that can be extended to coupled simulations involving heat transfer, mass transfer, and fluid flow in porous media.

2 Experimental

2.1 Sample preparation

The sample selected for this study is the core of a RPU sandwich insulation material. The sandwich insulation board sample was purchased from Langfang Changyexin Insulation Materials Sales Co., Ltd. The selected sandwich insulation board complied with the national standard GB/T 23923 and the industry standard JG/T 314-2012. The top and bottom surfaces of the sample were covered with 0.4 mm thick cement mortar paper (CMP), and the RPUc was 20 mm thick. The CMP covering layer was dark gray, whereas the RPUc was pale yellow. The density of the RPUc was approximately 50 $kg \cdot m^{-3}$, with a thermal conductivity of 0.026 $W \cdot m^{-1} \cdot K^{-1}$. The dimensions of the sample were 600 mm×1200 mm. The geometric structure of the sandwich insulation board sample and the physical board material are shown in Fig. 1.

During sample preparation, the covering layers were removed to isolate the RPU core. The RPUc was subsequently scraped into powder using a blade to obtain thermally thin samples suitable for milligram-scale thermal analysis. Prior to thermogravimetric analysis (TGA) and differential scanning calorimetry (DSC) tests, all the prepared samples were conditioned in a drying oven at 60 °C for 48 hours to eliminate residual moisture in the porous foam structure that could interfere with the microscale thermal characterization.

2.2 Simultaneous thermal analysis

A Netzsch STA449 F5 Jupiter simultaneous thermal analyzer (STA) was used to perform TGA and DSC tests on RPUc. Platinum-rhodium crucibles were selected for the experiments to ensure high sensitivity in heat flow data collection. The STA instrument was calibrated for temperature and sensitivity prior to the experiment to ensure accuracy. Since CMP is an inorganic material that does not participate in combustion reactions (under undamaged conditions, it isolates external oxygen from the combustible foam core), and the oxygen concentration in the thermal decomposition region of the material core tends toward zero under the influence of flames[25], nitrogen was purged into the thermal decomposition chamber of the STA instrument at a flow rate of 70 $mL \cdot min^{-1}$ during the STA tests to provide an inert atmo-

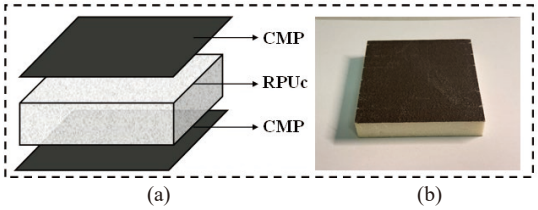


Fig. 1. Geometric structure diagram and real-panel diagram of RPU sandwich panels.

CSTR: 32290.14.JUSTC-2025-0084
DOI: 10.52396/JUSTC-2025-0084
JUSTC, **2026**, 56(X):

JUSTC Accepted

sphere for thermal degradation for RPUc.

The STA testing procedure was as follows[26, 27]: (1) A high-precision balance with a precision of 0.1 μg was used to initially weigh 5–10 mg of powdered flake samples. (2) To prevent the sample from flying out during movement and heating, the sample was placed in a platinum-rhodium crucible with a lid containing a 0.25 mm vent hole. During heating, the pyrolysis gases can escape through these small holes. (3) The sample and reference (empty) crucibles were placed symmetrically in the STA holder. (4) The sample was heated from 323 K to 973 K at heating rates of 5 K·min^{-1}, 10 K·min^{-1}, and 20 K·min^{-1} to obtain information on mass loss and heat flow evolution as functions of temperature. A blank test was conducted prior to each formal test to eliminate the influence of environmental factors on the test results.

The experimental data acquisition protocol recorded mass loss (m) and heat flow (HF) values at 1 K intervals throughout the heating program. From these primary measurements, derived parameters, including the mass loss rate (MLR) and integrated heat flow (IHF), were calculated as functions of temperature. All tests were repeated a minimum of three times, with the final results presented as the mean of repeated measurements. The error bars were calculated as two standard deviations of the mean, corresponding to an approximately 95% confidence interval for the reported data, which was plotted alongside the experimental data in these figures. For details, please refer to Sections 3.1 and 3.2.

3 Numerical model framework

3.1 Inverse modeling

Inverse modeling is a computational approach used to determine model input parameters on the basis of experimental results. This method is widely applied in parameter estimation, model calibration, and optimization. In general, the modeling process begins with the development of a forward model. Initial estimates of the input parameters are assumed, and the simulated results are compared with the experimental data. On the basis of the constructed mathematical model, the input parameters are iteratively optimized to obtain an optimal parameter set for the given materials and conditions, thereby developing a complete numerical model.

3.2 Governing equations

Since the material was prepared into a powdered thermally thin sample and the thermal analysis experiments were conducted at the milligram scale, the sample temperature can be assumed to instantaneously follow the programmed temperature of the furnace. Therefore, the reaction engineering model is reduced to a zero-dimensional heat-and-mass-transfer model because of negligible internal thermal gradients. The specific governing equations of the model are shown in Eqs. 1 to 4, which primarily include the energy conservation equation, mass conservation equation, Arrhenius reaction rate equation, and reaction scheme equation.

$$\frac{d\xi_j}{dt} = \sum_{i=1}^{N_r} \theta_i^j r_i \tag{1}$$

$$\sum_{j=1}^{N} \xi_j c_j \frac{dT}{dt} = \sum_{i=1}^{Nr} h_i r_i \tag{2}$$

$$r_i = A_i exp\left(-\frac{E_i}{RT}\right)\xi_{COMP1}\xi_{COMP2} \tag{3}$$

$$\theta_i^1 COMP1 + \theta_i^2 COMP2 \rightarrow \theta_i^3 COMP3 + \theta_i^4 COMP4 + h_i \tag{4}$$

In the governing equations, T denotes temperature (K), and t represents time (s), where N and N_r correspond to the total number of condensed-phase components and pyrolysis reactions in the reaction mechanism, respectively. The subscripts/superscripts i and j indicate the i-th reaction and j-th condensed-phase component, respectively. The key parameters include ξ_j for the mass concentration of the j-th condensed-phase component (kg·m^{-3}), θ_i^j as the stoichiometric coefficient of the j-th component in the i-th reaction, r_i for the reaction rate of the i-th reaction (kg·m^{-3}·s^{-1}), and c_j for the specific heat capacity of the j-th component (J·kg^{-1}·K^{-1}). The thermal parameters include the heat of pyrolysis for the i-th reaction (h_i, J·kg^{-1}), the Arrhenius pre-exponential factor (A_i, s^{-1}), and the activation energy (E_i, J·mol^{-1}), with R being the ideal gas constant (8.314 J·mol^{-1}·K^{-1}). The components are designated $COMP1$, $COMP2$(reactants) and $COMP3$, $COMP4$ (products), where ξ_{COMP1} and ξ_{COMP2} represent the mass concentrations of reactants 1 and 2 (kg·m^{-3}), respectively.

3.3 Modeling setup

Since the development of this model is based on numerical inversion using STA test values, the external heating boundary conditions of the model must correspond to the actual heating rate of the STA tests. As is well known, temperature transfer exhibits a time delay. Although the nominal heating rates were set at 5, 10, and 20 K·min^{-1} in the STA instrument, the real-time heating profiles exhibited dynamic variations because of inherent thermal inertia effects. As demonstrated by the experimental data points (blue, purple, and cyan scatter points in Fig. 2), the experimental heating rate initially increases but then gradually decreases before stabilizing at the target heating rate.

In this work, an appropriate exponential decay trigonometric function fitting function was adopted as the external heating condition input for the external heating boundary condition of the model, as expressed in Eq. 5 below.

$$\frac{dT}{dt}(t) = u_1\{1 - [exp(-u_2 t)][cos(u_3 t) + u_4 sin(u_3 t)]\} \tag{5}$$

In this equation, $\frac{dT}{dt}(t)$ represents the evolution of the instantaneous heating rate over time, where u_1, u_2, u_3, and u_4 denote the four fitting coefficients. The optimized coefficients for the three heating rates (5, 10, and 20 K·min^{-1}) are shown in Table 1. A comparison between the fitted values and experimental values of the heating rate is shown in Fig. 2, revealing excellent agreement. The R^2 value for the fitted data at 5 K·min^{-1} is 0.96, that at 10 K·min^{-1} is 0.96, and that at 20 K·min^{-1} is 0.97.

JUSTC Accepted

CSTR: 32290.14.JUSTC-2025-0084
DOI: 10.52396/JUSTC-2025-0084
JUSTC, **2026**, 56(X):

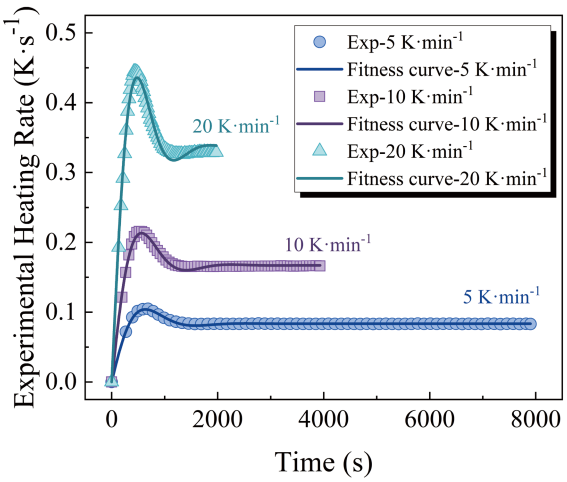


Fig. 2. STA heating rates and fitting curves.

Table 1. Fitting coefficients of the STA experimental heating rates.

Heating rate	u_1	u_2	u_3	u_4
5 K·min^{-1}	0.08353	0.002122	0.003316	−0.5018
10 K·min^{-1}	0.1671	0.002239	0.003727	−0.5432
20 K·min^{-1}	0.3357	0.002471	0.004547	−0.491

4 Results and Discussion

4.1 Characterization of the pyrolysis kinetics of RPUc

The m/m_0 and *MLR* of the sample as a function of temperature at a heating rate of 10 K·min^{-1} are shown in Fig. 3. All the data have been normalized by the initial mass to facilitate the observation and analysis of mass loss in RPUc at different pyrolysis stages. The error bars are visually negligible because of excellent experimental reproducibility, with their magnitudes comparable to the data point symbols. On the basis of the TGA profiles, the RPUc pyrolysis process can be categorized into three distinct stages:

(i) Initial decomposition stage (375–525 K): The cleavage of macromolecular bonds yields small molecular fragments with limited gas evolution.

(ii) Primary pyrolysis stage (525–750 K): Intensive degradation occurs, with rapid mass loss dominated by substantial volatile release.

(iii) Carbonization stage (750–900 K): The porous polymer matrix skeleton decomposes and collapses to form loose fibrous charcoal, with a residual carbon yield of 28.1%.

The *MLR* curve reveals five distinct peaks at 415 K (7.13×10^{-5} s^{-1}), 482 K (1.46×10^{-4} s^{-1}), 610.3 K (1.11×10^{-3} s^{-1}), 676.3 K (3.49×10^{-4} s^{-1}), and 798 K (1.42×10^{-4} s^{-1}), indicating that a five-step consecutive first-order lumped reaction mechanism is required to fully characterize the mass loss behavior of RPUc, as systematically presented in Table 2. The stoichiometric coefficients (θ) for each lumped pyrolysis reaction were derived from the *MLR* of RPUc using Eq. 6, while the corresponding reaction rates followed the Arrhenius formula (Eq. 3). Using Eqs. 7 and 8 in conjunction with the inverse modeling approach, initial estimates of the Arrhenius pre-exponential factor (A) and activation energy (E) for each reaction were obtained. These initial values were subsequently refined via a hill-climbing optimization algorithm [27]. On the basis of the developed numerical pyrolysis reaction model, the algorithm operates by iteratively adjusting the input parameters (θ, A, and E) in small increments and then searches for local optima while the simulated results are continuously compared with the experimental data. This process is repeated until a global optimum is achieved. Throughout the optimization, the goodness of fit (*GOF*) was evaluated using Eq. 9 and was iteratively updated until a predefined convergence criterion was satisfied. The final optimized values of θ, A, and E are presented in Table 2.

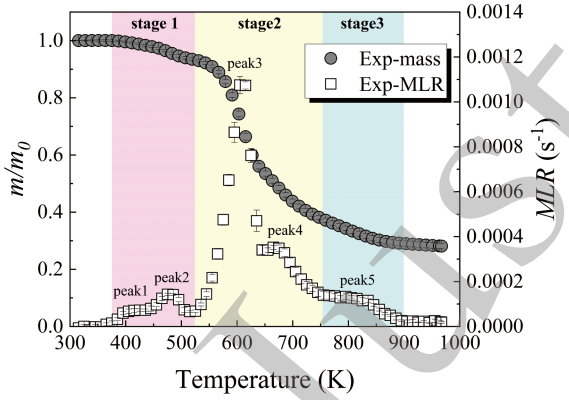


Fig. 3. TGA experimental data: m/m_0 and *MLR* profiles.

$$\theta_{c,i} = \frac{1-\sum_{n=1}^{n}\alpha_i}{\prod_{i=1}^{i-1}\theta_{c,i}}, (i>1) \tag{6}$$

$$A = \frac{eMLR_p}{m_{init}} exp\left(\frac{E}{RT_p}\right) \tag{7}$$

$$E = \frac{eRT_p^2 \frac{MLR_p}{m_{init}}}{(1-\theta)\frac{dT}{dt}} \tag{8}$$

Table 2. RPUc reaction mechanism of the pyrolysis model.

Serial number	Pyrolysis reaction	A (s^{-1})	E (J·mol^{-1})
1	RPUc→0.991 RPUc_int1+0.009 RPUc_gas1	3.39×10^{9}	8.81×10^{4}
2	RPUc_int1→0.939 RPUc_int2+0.061 RPUc_gas2	5.31×10^{2}	4.66×10^{4}
3	RPUc_int2→0.653 RPUc_int3+0.347 RPUc_gas3	7.02×10^{9}	1.39×10^{5}
4	RPUc_int3→0.637 RPUc_int4+0.363 RPUc_gas4	1.07×10^{1}	4.67×10^{4}
5	RPUc_int4→0.715 RPUc_res+0.285 RPUc_gas5	1.75×10^{-1}	3.15×10^{4}

Just Accepted

CSTR: 32290.14.JUSTC-2025-0084
DOI: 10.52396/JUSTC-2025-0084
JUSTC, **2026**, 56(X):

$$GOF = 1 - \frac{1}{Exp_{max}} \sqrt{\frac{\sum_{k=1}^{n} (Exp_k - Model_k)^2}{n}} \quad (9)$$

Here, $\theta_{c,i}$ represents the stoichiometric coefficient of the component of the condensed-phase product component of the i-th reaction, and α_i corresponds to the mass loss conversion rate associated with each lumped reaction. The subscript p denotes the value or corresponding temperature of the *MLR* peak, and m_{init} represents the initial mass of the RPUc sample. The symbol e refers to the base of the natural logarithm, and R is the universal gas constant. The *GOF* in the optimization algorithm is defined as follows: Exp_{max} indicates the maximum experimental value, Exp_k indicates the k-th experimental data point, $Model_k$ represents the simulated value at the k-th data point, and n is the total number of data points.

In this lumped pyrolysis reaction scheme, RPUc represents the original component. RPUc_int1 through RPUc_int4 correspond to four condensed-phase intermediate products formed during the reaction process, whereas RPUc_gas1 to RPUc_gas5 denote five gaseous pyrolysis products generated in the reaction. RPUc_res represents the final condensed-phase residual char component. Notably, owing to the inherent complexity of polymer chemical reactions, the defined components in the lumped reactions do not represent specific chemical substances but rather serve as collective representations encompassing multiple compounds. Nevertheless, the constructed lumped pyrolysis reaction mechanism successfully reproduces and predicts the critical thermal degradation characteristics of RPUc (including mass loss and heat flow data, as demonstrated in this work), thereby providing a sufficient theoretical foundation for material pyrolysis analysis.

The experimental and simulated TGA results under a 10 K·min^{-1} heating rate are compared in Fig. 4, where the red solid line represents the TGA simulation output from the pyrolysis reaction model. The results demonstrate that the proposed reaction framework, combined with optimally inverted input parameters, accurately reproduces the global pyrolysis behavior of RPUc. The model precisely captures (1) the pyrolysis onset temperature, (2) the three characteristic decomposition stages, (3) the peak magnitudes and positions of the *MLR*, and (4) the final char yield—all critical features of the thermal degradation process.

4.2 Characterization of the pyrolysis thermodynamics of RPUc

The mean of the experimental DSC data for RPUc are shown in Fig. 5, revealing the evolution of both the normalized *HF* and *IHF* with temperature. The results indicate that the *HF* curve exhibits three distinct thermal peaks, comprising two endothermic peaks and one exothermic peak. The specific positions and peak values are as follows: (1) 346 K, 0.163 W·

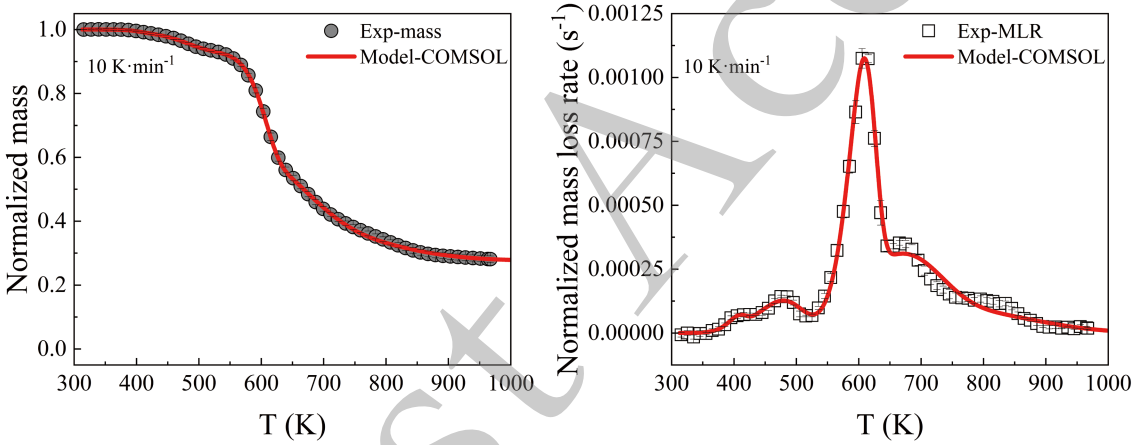


Fig. 4. Experimental and simulated TGA data at a heating rate of 10 K·min^{-1}.

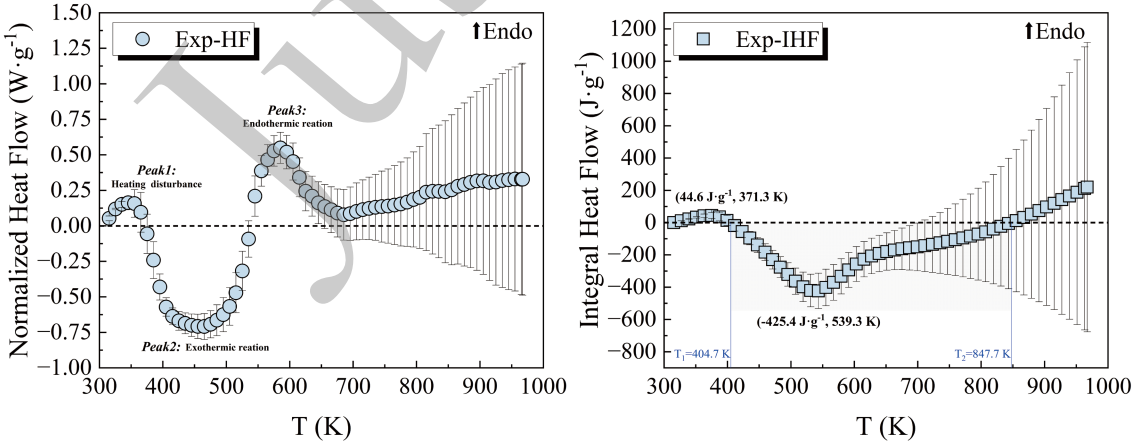


Fig. 5. DSC experimental data: Normalized heat flow and integral heat flow curves.

Just Accepted

CSTR: 32290.14.JUSTC-2025-0084
DOI: 10.52396/JUSTC-2025-0084
JUSTC, **2026**, 56(X):

g^{-1}; (2) 461 K, −0.711 $W \cdot g^{-1}$; and (3) 584 K, 0.549 $W \cdot g^{-1}$, where positive values denote endothermic processes and negative values represent exothermic processes, as indicated by the "Endo" direction in the figure. The first endothermic peak observed between 313 and 375 K arises from initial heating disturbances. The exothermic and endothermic peaks within 375–525 K result from pyrolysis-induced heat effects. Notably, the correlation with mass loss data from the TGA tests indicates that each *HF* peak corresponds to an *MLR* peak, definitively suggesting the absence of melting behavior during RPUc pyrolysis. The *IHF* curve initially increases to 44.6 $J \cdot g^{-1}$ at 371.3 K, after which it decreases from 371.3–539.3 K and then increases again with increasing temperature. The *IHF* remains negative within the temperature range of 407.7–847.7 K.

As expressed in Eq. 10, the total heat flow comprises two parts: sensible heat from temperature elevation and heat from pyrolysis reactions during RPUc pyrolysis. The initial mass of the sample (m_0), heat flow ($\dot{q}$), number of condensed-phase components (N_c), number of lumped pyrolysis reactions (N_r), mass concentration of the j-th component (ξ_j), volume (V), and Arrhenius reaction rate (r_i) are known. Consequently, accurate simulation of the total heat flow evolution requires precise determination of three key parameters: (i) the specific heat capacities of all condensed-phase components ($c_{p,j}$), (ii) the real-time instantaneous heating rates (dT/dt), and (iii) the reaction enthalpies associated with each lumped pyrolysis step ($h_{r,i}$).

$$\frac{\dot{q}}{m_0} = \sum_{j=1}^{N_c} \frac{V}{m_0} \xi_j c_{p,j} \frac{dT}{dt} + \sum_{i=1}^{N_r} \frac{V}{m_0} r_i h_{r,i} \tag{10}$$

The specific heat capacity of the initial component (RPUc) was determined by dividing the total DSC heat flow in the 315–332 K temperature range by the product of the instantaneous heating rate and sample mass. A polynomial function derived from linear fitting of this curve was adopted as the temperature-dependent input for the model. For the residual char component (RPUc_res), a value of 1700 $J \cdot kg^{-1} \cdot K^{-1}$ was assumed on the basis of literature-reported averages for polymeric chars[28]. On the basis of the specific heat capacities of RPUc and RPUc_res, in combination with the thermal decomposition mass loss curve, reasonable determinations were made for the specific heat capacities of each component of the intermediate products (RPUc_int1 to RPUc_int4) in the condensed phase (see detailed assignments in Table 3).

Table 3. Heat capacity of each condensed component.

Condensed component	c_p ($J \cdot g^{-1} \cdot K^{-1}$)
RPUc	444.17+1.52 T
RPUc_int1	444.17+1.14 T
RPUc_int2	444.17+0.76 T
RPUc_int3	444.17+0.76 T
RPUc_int4	444.17+0.76 T
RPUc_res	1700

The determined specific heat capacity was input into the pyrolysis reaction model framework, and the reaction heat of each lumped pyrolysis reaction was set as 0 in the model. The temperature rise sensible heat baseline could subsequently be output, as shown in Fig. 6. The three shaded areas in the figure quantitatively represent the heat of the pyrolysis reaction of the sample. The blue shaded area represents the net exothermic process, and the red shaded area represents the net endothermic process. Through iterative numerical inversion and optimization of the reaction model, the enthalpies for each lumped pyrolysis reaction were precisely determined (see complete parameterization in Table 4).

The pyrolysis reaction model framework developed for RPUc, incorporating the determined kinetic parameters, specific heat capacities of condensed phases, and heat of lumped pyrolysis reactions, successfully reproduces the experimental DSC data of RPUc. Fig. 7 demonstrates good overall agreement between the simulated heat flow curves and DSC experimental data, with only slight deviations observed: a minor overestimation of the initial exothermic peak and a small underestimation in the high-temperature region above 850 K. These discrepancies are considered to be caused by (i) the inherent complexity of pyrolysis mechanisms in polymeric materials and (ii) the diminished thermal sensitivity of STA at elevated temperatures, as evidenced by the larger error bars in the high-temperature range. The *IHF* curves derived from the temporal integration of both the experimental and simulated data strongly correspond, further validating the accuracy of the pyrolysis reaction model.

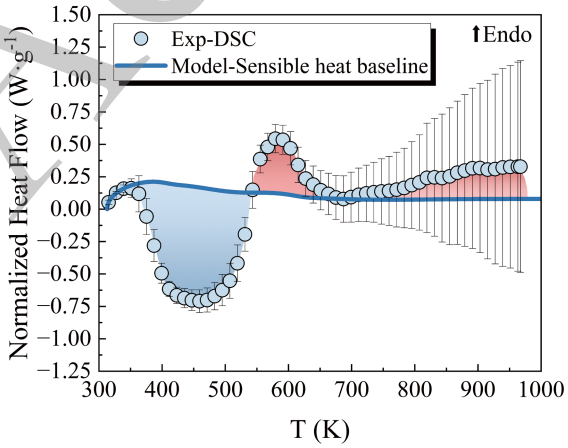


Fig. 6. Normalized heat flow data collected from the DSC tests and simulated sensible heat baseline.

Table 4. Heat of reaction of each first-order lumped pyrolysis reaction model.

Pyrolysis reaction	h_r ($J \cdot g^{-1}$)
1	53930.0
2	405746.9
3	−156311.6
4	−26881.0
5	−251436.9

Just Accepted

CSTR: 32290.14.JUSTC-2025-0084
DOI: 10.52396/JUSTC-2025-0084
JUSTC, **2026**, 56(X):

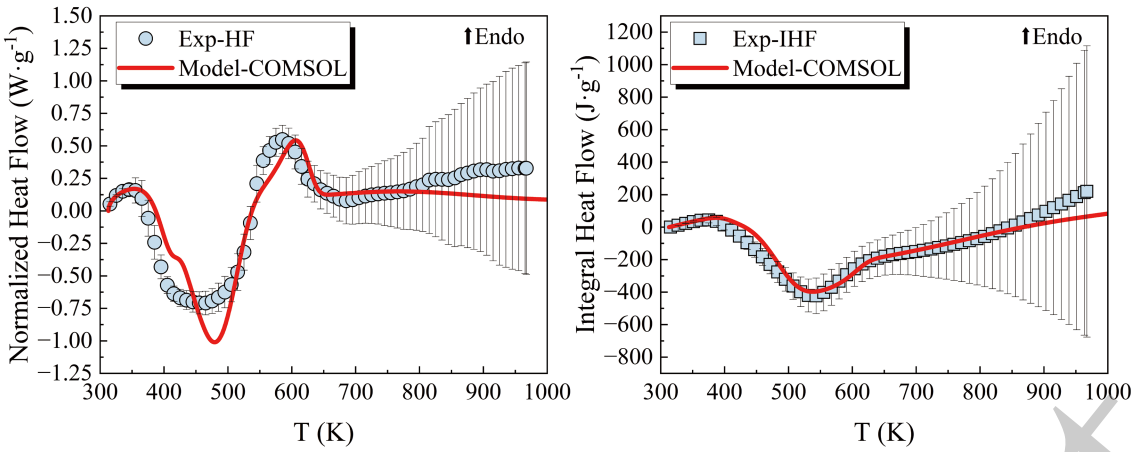


Fig. 7. DSC experimental and simulated data at a heating rate of 10 K·min^{-1}.

4.3 Pyrolysis reaction model validation

The pyrolysis reaction model developed in this work was applied to predict the mass loss behavior of RPUc under different heating conditions. In most kinetic studies[29–31] on polyurethane pyrolysis, the most commonly employed heating rate range is 0–20 K·min^{-1}. Therefore, the external heating parameters of the model were modified (using Eq. 5) to simulate both lower (5 K·min^{-1}) and higher (20 K·min^{-1}) heating rate conditions, with the simulation results compared against experimental TGA data for mutual validation in this work. In Fig. 8, the experimental TGA results are represented by scatter points with black-bordered circles for 5 K·min^{-1} and black-bordered squares for 20 K·min^{-1}, whereas the corresponding model simulation results are shown as solid red lines for 5 K·min^{-1} and 20 K·min^{-1}. As emphasized by the ICTAC Kinetics Committee in its guidelines for multi-step kinetic analysis[32], optimal kinetic parameters determined within a defined range may be reliably applied for interpolation and extrapolation, provided that the reaction mechanism remains essentially unchanged. In support of these conditions, a previous study[33] revealed that the pyrolysis mechanism of RPU does not significantly change even at relatively high heating rates. The excellent agreement between the simulated and experimental data across various heating rates confirms that the developed pyrolysis reaction model, through appropriate extrapolation, demonstrates a predictive capability over an extended range of thermal conditions.

5 Conclusions

The pyrolysis process of the RPUc was systematically investigated through STA, including the evolution of mass loss and heat flow. On the basis of the STA experimental data, the pyrolysis kinetics and thermodynamics were determined to develop a pyrolysis reaction model for predicting the behavior of RPUc pyrolysis under different heating conditions. The major findings are as follows:

(Ⅰ) Three distinct pyrolysis stages were identified: initial decomposition (375–525 K), primary pyrolysis (525–750 K), and carbonization (750–900 K). The majority of mass loss occurred during the primary pyrolysis stage, yielding a final char residue of 28.1%. Five *MLR* peaks were observed throughout the thermal decomposition stage, further confirming the complexity of the reaction mechanism of this RPUc polymer material.

(Ⅱ) Three significant *HF* peaks were resolved in the DSC measurements: an initial temperature-perturbation endotherm, followed by an exothermic peak and a subsequent endothermic peak. The *IHF* curve remained negative within the temperature range of 407.7–847.7 K, indicating the transition from net exothermic to net endothermic behavior.

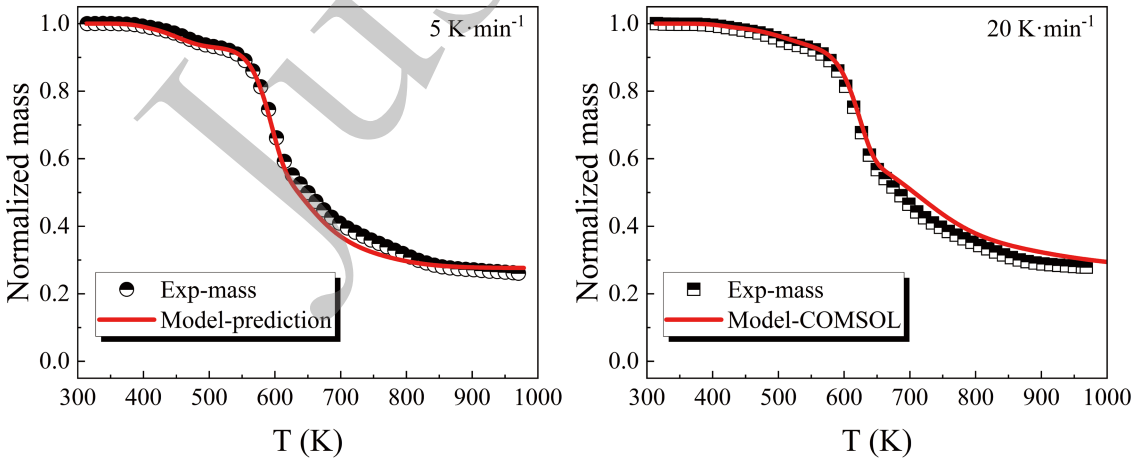


Fig. 8. Experimental and simulated TGA data at heating rates of 5 K·min^{-1} and 20 K·min^{-1}

Just Accepted

CSTR: 32290.14.JUSTC-2025-0084
DOI: 10.52396/JUSTC-2025-0084
JUSTC, **2026**, 56(X):

(Ⅲ) On the basis of the COMSOL Multiphysics reaction engineering model framework, five consecutive first-order thermal decomposition reactions were applied as the thermal decomposition reaction mechanism of RPUc, successfully capturing its thermal decomposition mass loss behavior. By changing the external heating conditions of the model, the TGA test results under different heating rates (5 $K \cdot min^{-1}$ and 20 $K \cdot min^{-1}$) were accurately predicted, verifying the predictive ability of the constructed reaction mechanism within a wide heating rate range.

(Ⅳ) The total heat flux during the RPUc pyrolysis process was simulated by coupling the sensible heat and the heat of the pyrolysis reaction. The specific heat capacity, heat of reaction, and instantaneous temperature increase rate, combined with the reaction mechanism kinetic framework, were used to successfully predict the *HF* and *IHF* curves, resulting in the development of a complete RPUc pyrolysis reaction model. This provides a critical pyrolysis characteristic input parameter set and a sub-model framework essential for developing comprehensive multi-dimensional pyrolysis models. Furthermore, the proposed systematic methodology is applicable for characterizing the pyrolytic behavior of flammable solids in flame-retardant sandwich panels and multi-layer polymer materials.

Acknowledgments

This work was supported by the National Natural Science Foundation of China (52506172), the National Key R&D Program of China (2022YFC3003102), the National High-Level Talent Youth Project (GG2320007006), the National Foreign Experts Program (S20240148), USTC Research Funds of the Double First-Class Initiative (YD2320002009) and USTC Start Research Funding (KY2320000046 & KY2320000055).

Conflict of Interest

The authors declare that they have no conflicts of interest.

Biographies

Xinyang Wang is pursuing a Ph.D. degree at the University of Science and Technology of China. His research mainly focuses on the fire safety of sandwich panels in construction with polymeric foam cores.

Xiaoyu Ju is currently a Special Professor at the State Key Laboratory of Fire Science, University of Science and Technology of China (USTC). He received his Ph.D. degree in Safety Science and Engineering from USTC in 2019. His research mainly focuses on fire prevention and control technologies for buildings, new energy systems (photovoltaic, wind power, etc), energy storage batteries, and underground spaces.

References

[1] Kannan N, Vakeesan D. Solar energy for future world: - A review. *Renewable and Sustainable Energy Reviews*, **2016**, *62*: 1092–1105.
[2] Wang Y, Guo C H, Du C, et al. Carbon peak and carbon neutrality in China: Goals, implementation path, and prospects. *China Geology*, **2021**, *4*: 720–746.
[3] Yang S, Yang D, Shi W, et al. Global evaluation of carbon neutrality and peak carbon dioxide emissions: Current challenges and future outlook. *Environmental Science and Pollution Research*, **2023**, *30*: 81725–81744.
[4] Professional Committee of Building Energy and Emissions, CABEE. Research Report on Carbon Emission in the Field of Urban and Rural Development in China (2024). 2024. https://cmsfiles.zhongkefu.com.cn/cmsossjianzhujieneng/upload/file/20250120/1737310863233732.pdf. Access May 10, 2025. (in Chinese)
[5] Lefebvre J, Bastin B, Le Bras M, et al. Flame spread of flexible polyurethane foam: Comprehensive study. *Polymer Testing*, **2004**, *23*: 281–290.
[6] Yu J, Yang C, Tian L, et al. A study on optimum insulation thicknesses of external walls in hot summer and cold winter zone of China. *Applied Energy*, **2009**, *86* (11): 2520–2529.
[7] Günther M, Lorenzetti A, Schartel B. Fire phenomena of rigid polyurethane foams. *Polymers*, **2018**, *10*: 1166.
[8] Hajduković M, Knez N, Knez F, et al. Fire Performance of External Thermal Insulation Composite System (ETICS) Facades with Expanded Polystyrene (EPS) Insulation and Thin Rendering. *Fire Technology*, **2017**, *53*: 173–209.
[9] Sun J, Hu L, Zhang Y. A review on research of fire dynamics in high-rise buildings. *Theoretical and Applied Mechanics Letters*, **2013**, *3*: 042001.
[10] Koohkan M, Dréan V, Girardin B, et al. Reconstruction of the Grenfell tower fire: Thermomechanical analysis of window failure during the Grenfell tower disaster. *Fire Technology*, **2021**, *57*: 69–100.
[11] Rodrigues M B B, Côrrea R, De Cademartori P H G, et al. Bio-based tannin foams: Comparing their physical and thermal response to polyurethane foams in lightweight sandwich panels. *Compounds*, **2024**, *4*: 1–16.
[12] Proença M, Garrido M, Correia J R, et al. Fire resistance behaviour of GFRP-polyurethane composite sandwich panels for building floors. *Composites Part B: Engineering*, **2021**, *224*: 109171.
[13] Proença M, Garrido M, Correia J R, et al. Experimental study on the fire resistance of all-composite and hybrid web-core sandwich panels for building floors. *Composite Structures*, **2024**, *337*: 118071.
[14] Wi S, Yang S, Yun B Y, et al. Fire retardant performance, toxicity and combustion characteristics, and numerical evaluation of core materials for sandwich panels. *Environmental Pollution*, **2022**, *312*: 120067.
[15] Feih S, Mathys Z, Gibson A G, et al. Modeling compressive skin failure of sandwich composites in fire. *Journal of Sandwich Structures & Materials*, **2008**, *10*: 217–245.
[16] Anjang A, Chevali V S, Lattimer B Y, et al. Post-fire mechanical properties of sandwich composite structures. *Composite Structures*, **2015**, *132*: 1019–1028.
[17] Anjang A, Chevali V S, Kandare E, et al. Tension modelling and testing of sandwich composites in fire. *Composite Structures*, **2014**, *113*: 437–445.
[18] Anjang A, Chevali V S, Feih S, et al. Deterioration of the fire structural resistance of sandwich composite under tension due to water absorption. *Composites Part A: Applied Science and Manufacturing*, **2016**, *87*: 263–270.
[19] Lautenberger C, Fernandez-Pello C. Generalized pyrolysis model for combustible solids. *Fire Safety Journal*, **2009**, *44*: 819–839.
[20] McGrattan K, Baum H, Rehm R, et al. Fire Dynamics Simulator: Technical Reference Guide (NISTIR 6467), NIST Interagency/Internal Report (NISTIR). Gaithersburg, MD, USA: National Institute of Standards and Technology, **2000**.
[21] Stoliarov S, Lyon R. Thermo-kinetic model of burning for pyrolyzing materials. *Fire Safety Science*, **2008**, *9*: 1141–1152.
[22] Stoliarov S I, Leventon I T, Lyon R E. Two-dimensional model of burning for pyrolyzable solids. *Fire and Materials*, **2014**, *38*: 391–408.
[23] Jiang L, Berto F, Zhang D. Pyrolysis kinetics and flammability evaluation of rigid polyurethane with different isocyanate content. *Molecules*, **2021**, *26*: 2386.

Just Accepted

CSTR: 32290.14.JUSTC-2025-0084
DOI: 10.52396/JUSTC-2025-0084
JUSTC, **2026**, 56(X):

[24] Zheng B, Li Y, Ma H, et al. Pyrolysis characteristics, kinetics and products of flexible polyurethane foam in luxury cruise ship *via* TG, FTIR, GC-MS and Shuffled Complex Evolution. *Journal of Analytical and Applied Pyrolysis*, **2024**, *179*: 106497.
[25] Korobeinichev O, Gonchikzhapov M, Tereshchenko A, et al. An experimental study of horizontal flame spread over PMMA surface in still air. *Combustion and Flame*, **2018**, *188*: 388–398.
[26] Wang X, Ding Y, Chen Z, et al. Measurement of the kinetics and thermodynamics of the thermal degradation for a flame retardant polyurethane-based aerogel. *Energies*, **2022**, *15*: 6982.
[27] Ding Y, Wang X, Zuo X, et al. Characterization of pyrolysis behavior for rigid polyurethane foam wastes with different densities through TGA-FTIR-DSC-MCC and Hill Climbing Optimization methods. *Journal of Analytical and Applied Pyrolysis*, **2024**, *177*: 106326.
[28] Ding Y, McKinnon M B, Stoliarov S I, et al. Determination of kinetics and thermodynamics of thermal decomposition for polymers containing reactive flame retardants: Application to poly(lactic acid) blended with melamine and ammonium polyphosphate. *Polymer Degradation and Stability*, **2016**, *129*: 347–362.
[29] Jiao L, Xiao H, Wang Q, et al. Thermal degradation characteristics of rigid polyurethane foam and the volatile products analysis with TG-FTIR-MS. *Polymer Degradation and Stability*, **2013**, *98*: 2687–2696.
[30] He J J, Jiang L, Sun J H, et al. Thermal degradation study of pure rigid polyurethane in oxidative and non-oxidative atmospheres. *Journal of Analytical and Applied Pyrolysis*, **2016**, *120*: 269–283.
[31] Zeller M, Garbev K, Weigel L, et al. Thermogravimetric studies, kinetic modeling and product analysis of the pyrolysis of model polymers for technical polyurethane applications. *Journal of Analytical and Applied Pyrolysis*, **2023**, *171*: 105976.
[32] Vyazovkin S, Burnham A K, Favergeon L, et al. ICTAC Kinetics Committee recommendations for analysis of multi-step kinetics. *Thermochimica Acta*, **2020**, *689*: 178597.
[33] Wang S, Chen H, Zhang L. Thermal decomposition kinetics of rigid polyurethane foam and ignition risk by a hot particle. *Journal of Applied Polymer Science*, **2014**, *131*: 39359.

Just Accepted

CSTR: 32290.14.JUSTC-2025-0084
DOI: 10.52396/JUSTC-2025-0084
JUSTC, **2026**, 56(X):